Selective-adsorption structures in the inelastic scattering of He-graphite (0001)

P. Cantini and R. Tatarek
Gruppo Nazionale di Struttura della Materia del Consiglio Nazionale delle Ricerche and Istituto di Scienze Fisiche dell'Università, Viale Benedetto XV, 5, 16132 Genova, Italy
(Received 29 April 1980)

Structures were observed in the angular distribution of helium atoms inelastically scattered by the graphite (0001) surface; they were clearly identified as bound-state resonance processes ("selective adsorption") assisted by phonons. To better understand the mechanism of the inelastic process, detailed measurements taken at different incident angles for the structure corresponding to a well-defined resonance are presented. Some unexpected behavior, as the change of shape and intensity of an inelastic resonance observed at definite incident angles, suggests the occurrence of multiple resonant transitions between different energy levels of the gas-surface potential. The experimental data are analyzed theoretically in terms of single-phonon inelastic processes, on the assumption of a model potential with a time-dependent short-range repulsion and a stationary long-range attraction. Explicit formulas for inelastic selective adsorption are obtained in the eikonal approximation, assuming a corrugate hard-wall repulsion. Different ways to go resonantly in a bound state are considered, with or without energy exchange with the surface. The calculated behavior of resonances shows reasonably good agreement with the experimental data on He-graphite. From the angular position of phonon-assisted resonances preliminary information on the graphite (0001) surface dynamics has been obtained, in agreement with calculated phonon spectra.

I. INTRODUCTION

The scattering of supersonic beams of light atoms from crystalline surfaces has reached remarkable interest as a tool for the study of gas-solid interactions and for the investigation of dynamic properties of surfaces. The study of elastic diffraction intensities recently demonstrated the power of this technique both to observe structural features of clean[1,2] or adsorbate-covered surfaces[3] and to obtain detailed informations on the gas-surface interaction potential through the selective adsorption resonances.[4–6] In addition, measurements of the inelastic scattering of thermal atoms with a detailed energy analysis of the scattered particles hold promise of providing a new tool for studying the dispersion curves of surface phonons.[7,8] Time-of-flight spectra can show (and recently showed[9]) sharp structures in the inelastic scattering, probably related to discrete surface modes.[10,11]

In addition, structures in the angular distribution of inelastically scattered particles can be related to inelastic selective adsorption resonances, a process that was observed in the past.[12–14] The present paper will report some new experimental results on this process, obtained for the scattering of He from the basal plane of graphite. A theoretical description will also be presented, in which the effects of resonances on the inelastic scattering are taken into account, in the single-phonon approximation.

When an atom of mass M and incident momentum $\vec{k}_0 = (\vec{K}_0, k_{0_z})$ collides with a periodic surface, the kinematic conditions for an inelastic process involving the creation of one phonon are

$$k^2 = k_0^2 - 2M\omega_q/\hbar \ , \tag{1.1}$$

$$\vec{K}_G = \vec{K}_0 + \vec{G} - \vec{Q} \ , \tag{1.2}$$

where $\vec{G}$ is a surface reciprocal-lattice vector and the created phonon has a parallel momentum $\vec{Q}$ and angular frequency ω_q [for annihilation processes the sign of both $\vec{Q}$ and ω_q in Eqs. (1.1) and (1.2) must be reversed].

A selective adsorption resonance occurs whenever a closed channel $\vec{N}$ exists, for which

$$k_{N_z}^2 = k^2 - K_N^2 \simeq 2M\epsilon_j/\hbar^2 \ , \tag{1.3}$$

ϵ_j being an energy level of the gas-surface averaged potential V_0. The resonance condition (1.3) can be fulfilled in a purely elastic way, when

$$2M\epsilon_N/\hbar^2 = k_0^2 - (\vec{K}_0 + \vec{N})^2 \simeq 2M\epsilon_j/\hbar^2 \ , \tag{1.4}$$

ϵ_N being the energy of the perpendicular motion of the atom. This "elastic resonance" occurs for selected $\vec{k}_0$'s and will affect the intensity of the elastic dif-

fraction peaks as well as the inelastic transition probability.

The condition (1.3) can also be satisfied after creation of one phonon, when:

$$2M\epsilon_{N-Q}/\hbar^2 = (k_0^2 - 2M\omega_q/\hbar) - (\vec{K}_0 + \vec{N} - \vec{Q})^2 \simeq 2M\epsilon_j/\hbar^2 \quad (1.5)$$

This "phonon-assisted" resonance occurs at any $\vec{k}_0$, for a family of phonons $\omega_{Nj}(\vec{Q})$ given by Eq. (1.5), and will affect the scattering processes involving these phonons.[13]

The effects of the elastic resonances on the intensity of diffraction peaks has been widely studied in the past years both by theoreticians[15–18] and by experimentalists.[4–6,19,20] The primary aim was to understand better the elastic scattering process. An elastic theory appeared as adequate to describe the resonance structures in the diffraction intensity; the computed shapes, linewidths, positions, and splittings were in overall agreement with detailed experimental results.[15–18,21] More recently the role of inelastic effects on the elastic resonances has been explored phenomenologically through a complex optical potential, and the agreement with the experimental data has been improved.[22–24]

Effects of elastic and inelastic resonances on the inelastic transition probability have been little studied until now. Experimental evidence of resonant structures in the inelastic scattering has been found only in a few cases,[13] where the angular distributions of the inelastic tails of specular peaks were studied at different incident angles θ_0 for He and Ne scattered by the (001) face of LiF. Since the resonance condition (1.5) selects different phonons $\omega_{Nj}(\vec{Q})$ at different θ_0, the angular position of resonances allowed an average phonon spectrum to be determined, in apparent agreement with the theoretical knowledge on the surface dynamics of LiF. However some uncertainty remained on the possibility of using inelastic resonances to determine univocally the phonon spectrum at the surface.[25] To understand better the proposed mechanism, we present here further measurements of resonances in the inelastic tails of He diffracted by graphite. The experimental data are given in Sec. II. The resonances of He-graphite show a behavior in some way new with respect to the previous observations on LiF; the structures in the inelastic tail, which at several incident angles show shapes similar to the resonances in the elastic intensity, suddenly change shapes at some definite incident angles. To explain this and other resonant effects we propose in Sec. III the main lines of a theoretical treatment for the single-phonon inelastic process which takes into account the attractive well of the gas-solid potential. The analysis of the data is then given in Sec. IV. Section V gives the conclusions.

II. EXPERIMENTAL RESULTS

The experimental setup was the same used in the study of elastic resonances.[5] Present data refer to scattering of a He beam produced with a nozzle source at 200 K; the atoms, with a wave vector $k_0 = 9.07$ Å^{-1} (and an energy $E_0 = 42.96$ meV) were scattered by the graphite basal plane at 80 K. In order to study the angular dependence of a well-defined inelastic structure we looked for a resonance associated with a closed channel strongly coupled to the specular, and appearing in a "free" region of the reciprocal space where no other resonances can interfere. We chose the $(j-10)-(j-01)$ crossing in the $\phi_0 = 30°$ azimuth; these resonances are coupled by the nonzero V_{10} Fourier component of the potential and two split energy levels $\epsilon_j^{\pm} = \epsilon_j \pm \langle j|V_{10}|j\rangle$ should be found. In this direction however, as noted by Chow,[26] only the symmetric combination of the two free-particle states contributes to the resonant transition. Hence only one resonance is seen at $\phi_0 = 30°$, at the position corresponding to the eigenvalue ϵ_j^+ of the potential $V_0 + V_{10}$. The intensity of the specular peak, as a function of θ_0, is shown in Fig. 1; four resonances are well identified, associated to the $\vec{N} = (10)$ and $\vec{N} = (01)$ closed channels; their angular positions correspond to the energy values $\epsilon_0^+ = -12.24$, $\epsilon_1^+ = -6.55$, $\epsilon_2^+ = -2.98$, and $\epsilon_3^+ = -1.06$ meV. These energy values agree with the previously measured energy levels and matrix elements.[5] A fifth resonance, corresponding to the energy $\epsilon_4^+ = -0.20$ meV, appears in Fig. 1 as completely smoothed at the experimental conditions. Following Chow,[26] the energy values ϵ_j^+ will be used hereafter as levels of the potential $V_0 + V_{10}$ to describe the $(j-10)-(j-01)$ crossing in the $\phi_0 = 30°$ azimuth (and will be indicated as ϵ_j for simplicity).

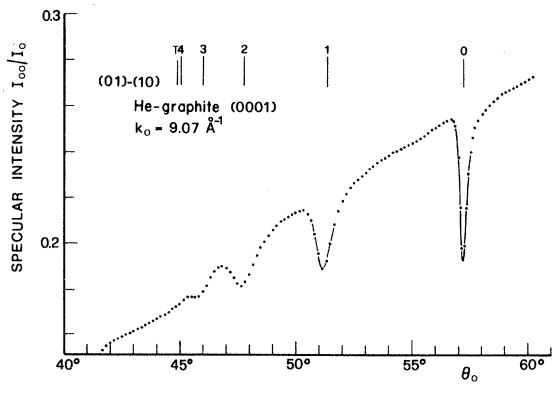

FIG. 1. Specular intensity at $\phi_0 = 30°$ vs incident angle. Vertical bars indicate shifted resonance positions, assuming the energy values $\epsilon_j^+ = \epsilon_j + V_{10}^{jj}$ as levels of the potential $V_0 + V_{10}$. Resonances are labeled by reciprocal-lattice-vector indices and by level index; T shows calculated location of the threshold.

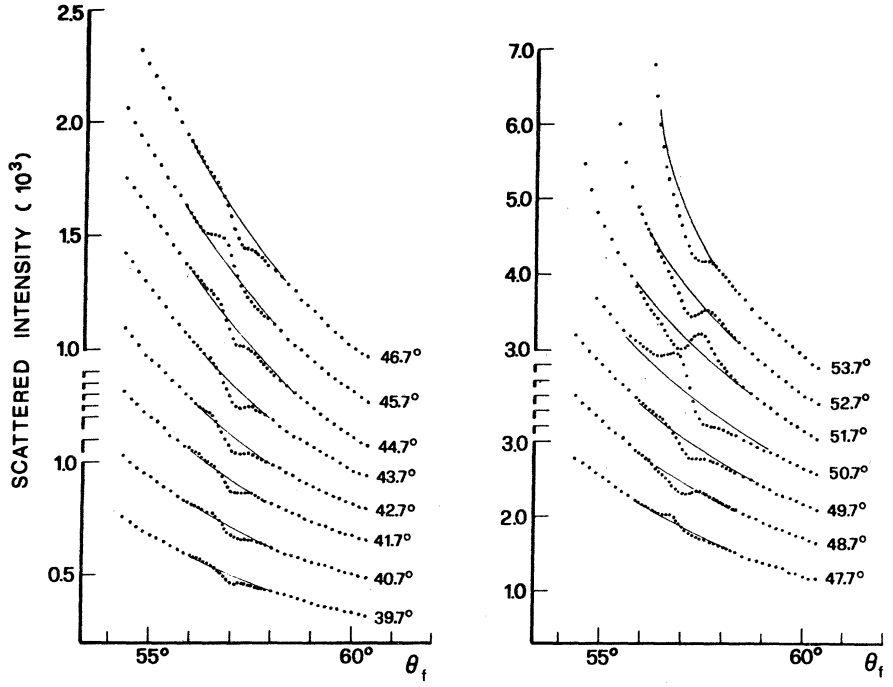

FIG. 2. In-plane angular distributions of the inelastic tail of the specular peak at different incident angles θ_0. The continuous line represents the estimated nonresonant inelastically scattered intensity.

As can be seen in Fig. 1, the minimum at $\theta_0 \simeq 57.2°$ is a very sharp structure, well suited to study resonances in the inelastic scattering. For this purpose the in-plane tail of the specular peak was analyzed as a function of the final angle $54° < \theta_f < 61°$, for about fifty incident angles $40° < \theta_0 < 55°$; many of the angular distributions are reported in Figs. 2, 3, and 4. In Fig. 2 the more relevant appearances of the resonance can be seen; a structure appears near $\theta_f \simeq 57°$, whose position changes very little with the incident angle and which clearly corresponds to the minimum at $\theta_0 = 57.2°$ in the specular intensity of Fig. 1. Because at these incident angles the resonance condition can be fulfilled only through Eq. (1.5), the structure can be identified as a phonon-assisted resonance and will be labeled $(0-10)-(0-01)$. The shape of the structure at several incident angles θ_0 is the same as the structure in the specular peak; it has a small shoulder followed, at larger θ_f, by a minimum which becomes deeper as θ_0 approaches 57.2°. However at particular incident angles the behavior is quite different, as at $\theta_0 \simeq 45.7°$, where the resonance appears as a large maximum, or at $\theta_0 \simeq 50.7°$ and $\theta_0 \simeq 51.7°$, where maxima and minima are present.

In Fig. 3 scans taken at many intermediate incident angles are reported, in a region where the resonance shape rapidly changes. At $\theta_0 \simeq 51.03°$ a strong maximum takes the place of the minimum, then again it decreases and disappears. A similar behavior is

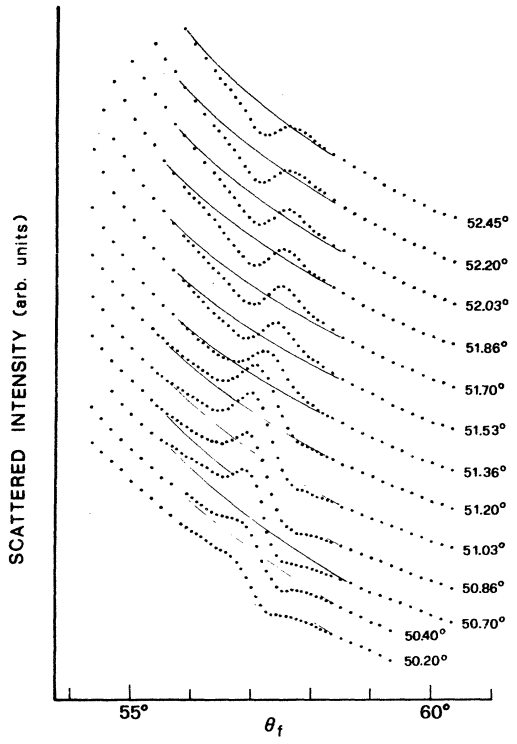

FIG. 3. Angular distributions similar to those of Fig. 2 for incident angles θ_0 near the elastic resonance labeled $(1-01)-(1-10)$ in Fig. 1.

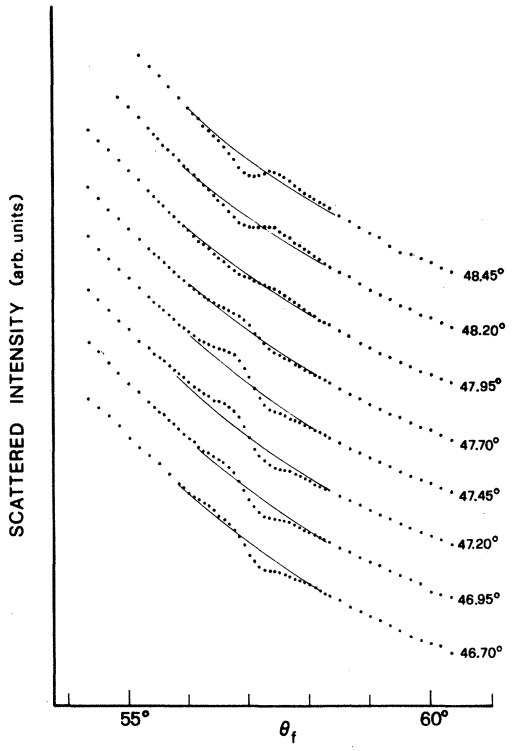

FIG. 4. Angular distributions similar to Fig. 3 at incident angles θ_0 near the elastic resonance labeled (2−01)−(2−10) in Fig. 1.

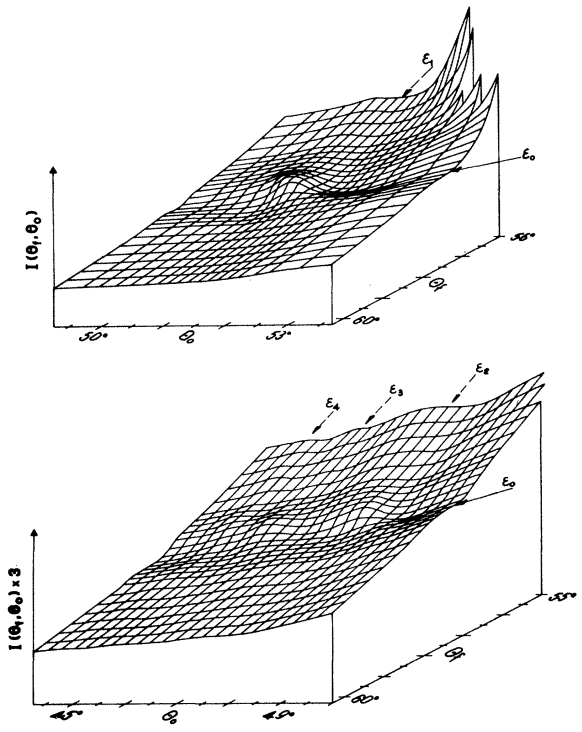

FIG. 5. Plot of the inelastically scattered intensity vs both the incident angle θ_0 and the final angle θ_f. Dashed arrows indicate elastic resonances at given θ_0's. Full arrow indicates phonon-assisted resonance.

shown in Fig 4, with a maximum on the angular distribution taken at $\theta_0 \cong 47.45°$.

It is easily found that maxima in the inelastic scattering occur at those incident angles where a new resonance appears in the intensity of the elastic peak (see Fig. 1). This effect is evident in Figs. 5(a) and 5(b) where the inelastic intensity $I(\theta_f, \theta_0)$ is reported as a function of both the incoming θ_0 and final angle θ_f; the elastic resonances [Eq. (1.4)] which affect the inelastic scattering are indicated by dashed arrows at $\theta_0 \simeq 45°$, $\theta_0 \simeq 45.9°$, $\theta_0 \simeq 47.7°$, and $\theta_0 \simeq 51.2°$; the phonon-assisted resonance (1.5) is indicated by a full arrow at $\theta_f \simeq 57.2°$. Both the elastic resonances at fixed incident angles and the inelastic resonance at a given final angle are minima; a similar behavior was observed also for He-LiF and Ne-LiF.[13]

When however the two conditions (1.4) and (1.5) are satisfied simultaneously, a large interference effect appears as a maximum in the $I(\theta_f, \theta_0)$. This effect is observed here for the first time. As will be discussed below, it can be explained as a double-resonance process, with an elastic transition to a bound state $(j - \vec{N})$ followed by an inelastic transition to a different bound state $(j' - \vec{n}')$, with $\vec{n}' = \vec{N} - \vec{Q}$. The maxima in Fig. 5 suggest a large probability for this inelastic transition between two different energy levels.

III. THEORETICAL FORMALISM

Among the recent elastic theories devoted to explain the selective adsorption phenomena,[15–18] the formalism developed by Celli, Garcia, and Hutchinson[18] appeared to us as the best suited to be extended to the inelastic scattering; we will follow as closely as possible this work, denoted henceforth as CGH.

The gas-surface potential is assumed to be of the type

$$V(\vec{r},t) = V_R(z - \zeta(\vec{R},t)) - V_A(z) \ , \qquad (3.1)$$

where V_R is a short-range repulsion, $\zeta(\vec{R},t)$ is an effective surface corrugation profile, here time dependent, and $V_A(z)$ is a long-range attraction. Notice that we assume a stationary attraction: this implies that the inelastic process takes place only when the gas-atom interacts with the V_R. Like CGH we assume that there are two planes, $z = z_0$ and $z = z_0 - \delta$,

with $\delta > 0$, such that

$$V_R(z-\zeta(\vec{R},t))=0 \quad \text{for } z > z_0-\delta \ , \tag{3.2a}$$

$$V_A(z)=-D \quad \text{for } z < z_0 \ . \tag{3.2b}$$

So the attractive well has a flat bottom of depth D, and a width δ arbitrarily small; we can solve separately for the wave functions of V_R and V_A, and then match at $z=z_0$.

The wave function in the intermediate region $z_0-\delta < z < z_0$ is given by a combination of plane waves of different energies E:

$$\psi_D(\vec{r},t)=\sum_k [b_k^+\phi_k^+(\vec{r},t)+b_k^-\phi_k^-(\vec{r},t)] \ , \tag{3.3}$$

with

$$\phi_k^{\pm}(\vec{r},t)=e^{i\vec{K}\cdot\vec{R}}e^{\pm ipz}e^{-i(E+D)t/\hbar} \ , \tag{3.4}$$

where $K^2+p^2=2M(E+D)/\hbar^2$ (we used k instead of $\vec{k}$ as a subscript for simplicity). The sum over $\vec{k}$ in Eq. (3.3) runs over all continuum states related to the initial state $\vec{k}_0$ by the usual conservation conditions for multiphonon inelastic processes. The plane waves (3.4) are also separately eigenstates of V_R-D and V_A for $z_0-\delta < z < z_0$.

The wave function in the vacuum ($z \to +\infty$) is

$$\psi(\vec{r},t)=\varphi_{k_0}^-(\vec{r},t)+\sum_k a_k\varphi_k^+(\vec{r},t) \ , \tag{3.5}$$

with

$$\varphi_k^+(\vec{r},t)=e^{i\vec{K}\cdot\vec{R}}e^{ik_z z}e^{-iEt/\hbar} \ , \tag{3.6}$$

where $K^2+k_z^2=2ME/\hbar^2$. The scattering problem is then to determine the coefficients a_k.

If now we assume that both the inelastic scattering problem at the repulsive wall V_R-D and the elastic scattering problem for V_A have been solved, then as a formal extension of Eq. (2.13) of CGH to the inelastic scattering we obtain the integral equation for b_k^+ coefficients

$$b_k^+=\mathcal{S}(\vec{k};\vec{k}_0)T_0'+\sum_{k'}\mathcal{S}(\vec{k},\vec{k}')R_{k'}b_{k'}^+ \ , \tag{3.7}$$

where $\mathcal{S}(\vec{k},\vec{k}')$ are the known scattering coefficients for elastic or inelastic interaction with V_R-D, while $R_{k'}$ and T_0' are reflection and transmission coefficients for V_A. When the integral equation (3.7) is solved for a given final state $\vec{f}=(\vec{K}_f,k_{f_z})$, the inelastic scattering probability is obtained as

$$\frac{dP(\vec{f},\vec{0})}{dEd^2\Omega}=|a_f|^2=\frac{p_f}{k_{f_z}}|b_f^+|^2 \ . \tag{3.8}$$

As expected from the assumed model potential [Eq. (3.1)], the inelastic scattering probability in the presence of an attractive well can be expressed in terms of the scattering coefficients $\mathcal{S}$ at V_R-D.

Till now we considered a multiphonon process. We are interested in considering only single-phonon processes as they are the most probable. To do this we suppose that the scattering coefficients at the potential V_R-D are very small for multiphonon processes; so we can substitute the coefficient $\mathcal{S}(\vec{K},E+D);\vec{K}',E'+D)$ in Eq. (3.7) with the elastic $S(\vec{K},E+D;\vec{K}+\vec{G}',E+D)$ and with the one-phonon $s(\vec{K},E+D;\vec{K}+\vec{G}'-\vec{Q}',E+D-\hbar\omega_q')$ coefficients. Moreover Eq. (3.7) could give multiphonon processes also as effect of multiple reflections inside the well; this effect is surely important, especially in the selective adsorption processes. However, being interested in single-phonon processes—[where the $(\vec{Q},\omega_q)$ of the phonon are completely identified through the initial and final state of the scattered atom]—we impose the kinematic conditions Eqs. (1.1) and (1.2). Equation (3.7) then becomes

$$b_{G-Q}^+=s(\vec{G}-\vec{Q},\vec{0})T_0' + \sum_{G'}[s(\vec{G}-\vec{Q},\vec{G}')R_{G'}b_{G'}^+ + S(\vec{G}-\vec{Q},\vec{G}'-\vec{Q})R_{G'-Q}b_{G'-Q}^+] \tag{3.9}$$

(we omitted for simplicity the energy E and the initial parallel momentum $\vec{K}_0$ in the notation of the scattering amplitude and in the subscript).

For any final state $\vec{f}=(\vec{F}-\vec{Q},E_0-\hbar\omega_q)$ Eq. (3.9) gives a matrix equation for b^+ which can be solved by the standard matrix algebra in a way completely similar to the elastic scattering problem. The general advantage of the single-phonon approximation is that the set of integral equations (3.7) is reduced to a set of linear equations; the same result was obtained by Manson and Celli[27] for the one-phonon scattering described in the t-matrix formalism. A full discussion of the validity limits of Eq. (3.9) is out of the aim of the present paper; here we want to show some of the most relevant effects of selective adsorption on inelastic scattering.

We recall[18] that for smoothly varying V_A the coefficients R_F for open channels $\vec{F}$ are very small; the summation in Eq. (3.9) can therefore be extended over $\vec{N}$ vectors only, namely, over the closed channels below the continuum threshold in the well, leading to possible resonances with bound states ($j-\vec{N}$). Let us assume that there is only one $\vec{N}$ vector, strongly coupled to the specular; through it the atom can go in a bound state either with an elastic or with an inelastic transition.

As a first example we consider the elastic resonance followed by creation of one phonon; for this process

$$b_N^+=S_{N0}T_0'(1-S_{NN}R_N)^{-1} \ , \tag{3.10}$$

with $S_{NN}=S(\vec{N},\vec{N})$. Following CGH a phase shift

$\delta(\epsilon_N)$ can be defined for $S_{NN}R_N$; thus

$$b_N^+ = \frac{ie^{-i\delta}S_{N0}T_0'}{(\epsilon_N - \epsilon_j + i\Gamma_N/2)\left(\frac{d\delta}{d\epsilon_N}\right)} , \quad (3.11)$$

where ϵ_N is given by Eq. (1.4). The coefficient b_N^+ is a typical resonance with a width

$$\Gamma_N = 2\left(\frac{d\delta}{d\epsilon_N}\right)^{-1}(1-|S_{NN}|) . \quad (3.12)$$

Then for a final state $\vec{f}$ Eq. (3.9) gives

$$b_f^+ = s_{f0}T_0' + \frac{ie^{-i\delta}s_{fN}R_NS_{N0}T_0'}{(\epsilon_N - \epsilon_j + i\Gamma_N/2)\left(\frac{d\delta}{d\epsilon_N}\right)} . \quad (3.13)$$

The inelastic scattering probability is obtained from Eq. (3.8) as

$$\frac{dP(\vec{f},\vec{0})}{dEd^2\Omega} - = I^0(\vec{f},\vec{0})|1+\frac{iB}{X+i}|^2 , \quad (3.14)$$

where $I^0(\vec{f},\vec{0}) = p_{f_z}k_{0_z}|s_{f0}|^2/p_{0_z}k_{f_z}$ is the single-phonon inelastic scattering probability, in the absence of multiple reflection inside the well, with $s_{gG'} = s(\vec{G}-\vec{Q},\vec{G}')$; $X = 2(\epsilon_N - \epsilon_j)/\Gamma_N$ and $B = s_{fN}R_NS_{N0}/s_{f0}(1-|S_{NN}|)$. In general we can approximate s_{fN}/s_{f0} with S_{fN}/S_{f0}, where $S_{gG'} = S(\vec{G}-\vec{Q},\vec{G}')$ is the elastic scattering amplitude, except that of course $\vec{G}-\vec{Q}$ is not restricted to be a reciprocal-lattice vector. For instance this can be done for a hard corrugated wall potential (HCW) for which the inelastic scattering amplitude can be written as[28]

$$s_{gG'} = S_{gG'}\{\rho_{zz}(\vec{Q},\omega_q)[n_\omega(\vec{Q})+1]\}^{1/2} , \quad (3.15)$$

where $\rho(\vec{Q},\omega_q)$ is a spectral density tensor for surface phonons and $n_\omega(\vec{Q})$ is the occupation number. Then B becomes

$$B \simeq S_{fN}R_NS_{N0}/S_{f0}(1-|S_{NN}|) . \quad (3.16)$$

This last expression, which is exact for a HCW, gives B as a smoothly varying function of $(\vec{Q},\omega_q)$. Thus the main result of this example is that, when an elastic resonance occurs ($\epsilon_N \simeq \epsilon_j$), both the intensity of the elastic peaks and the neighboring inelastic tails are modified in the same way. This effect was clearly observed in the scattering of Ne-LiF (Ref. 13); it appears also with He-graphite (see Fig. 5).

As a second example we consider the creation of one phonon followed by a resonance transition into a bound state; Eq. (3.9) gives for the closed channel

$$b_n^+ = \frac{is_{n0}T_0'R_n}{(\epsilon_n - \epsilon_j + i\Gamma_n/2)\left(\frac{d\delta}{d\epsilon_n}\right)} , \quad (3.17)$$

with in general $\vec{n} = \vec{N}-\vec{Q}$; the ϵ_n is given by Eq. (1.5). The inelastic scattering probability becomes

$$\frac{dP(\vec{f},\vec{0})}{dEd^2\Omega} = I(\vec{f},\vec{0}) = I^0(\vec{f},\vec{0})\left|1+\frac{iC}{x+i}\right|^2 , \quad (3.18)$$

with $x = 2(\epsilon_n - \epsilon_j)/\Gamma_n$ while from Eq. (3.15) the coefficient $C \simeq S_{fn}R_nS_{n0}/S_{f0}(1-|S_{nn}|)$ is a smoothly varying function of $(\vec{Q},\omega_q)$. Equation (3.18) clearly shows that at any incident condition the inelastic scattering can have a large resonant contribution for the phonons $\omega_{Nj}(\vec{Q})$ selected by Eq. (1.5). This is the phonon-assisted selective adsorption, which is responsible for the strong structures observed in the past for He-LiF and Ne-LiF.[13] In the limit of low-energy phonons $C \simeq B$, then the shape of inelastic resonances is similar in many cases to the corresponding structures in the intensity of elastic peaks. This behavior appears in Fig. 2 for He-graphite at several incident angles.

As a further interesting example we consider the case where both an elastic resonance in a level ϵ_j and an inelastic resonance in a different level $\epsilon_{j'}$ occur at the same time. Equation (3.9) gives two coupled equations for b_N^+ and b_n^+:

$$b_N^+ = S_{N0}T_0' + S_{NN}R_Nb_N^+ + s_{Nn}R_nb_n^+ , \quad (3.19a)$$

$$b_n^+ = s_{n0}T_0' + s_{nN}R_Nb_N^+ + S_{nn}R_nb_n^+ . \quad (3.19b)$$

The solution, neglecting second-order terms $s_{Nn}s_{n0}$ and $s_{Nn}s_{nN}$ which represent virtual phonon processes, gives

$$\frac{dP(\vec{f},\vec{0})}{dEd^2\Omega} = I^0(\vec{f},\vec{0})\left|1+\frac{iB}{X+i}+\frac{iC}{x'+i}+\frac{i^2B'}{(X+i)(x'+i)}\right|^2 , \quad (3.20)$$

with

$$B' = S_{fn}R_nS_{nN}R_NS_{N0}/S_{f0}(1-|S_{NN}|)(1-|S_{nn}|) ,$$

while $x' = 2(\epsilon_n - \epsilon_{j'})/\Gamma_n$. Thus the inelastic scattering probability contains a nonresonant term $I^0(\vec{f},\vec{0})$ modulated by three resonant contributions. $B/(X+i)$ corresponds to the elastic resonance transition in the level ϵ_j, which select the incidence condition $\vec{k}_0$ and affects the inelastic scattering for all the phonons; $C/(x'+i)$ corresponds to the inelastic resonance transition in the level $\epsilon_{j'}$ for the phonons $\omega_{Nj'}(\vec{Q})$ selected by Eq. (1.5). For these phonons the last term $B'/(X+i)(x'+i)$ gives a further resonant contribution, large when both the elastic and the phonon-assisted resonance are present; this corresponds to an elastic resonant transition $\vec{0}\rightarrow\vec{N}$ in the level ϵ_j followed by an inelastic resonant transition $\vec{N}\rightarrow\vec{n}$ to a different bound level ϵ_j' and is responsible for the large maxima observed with He-

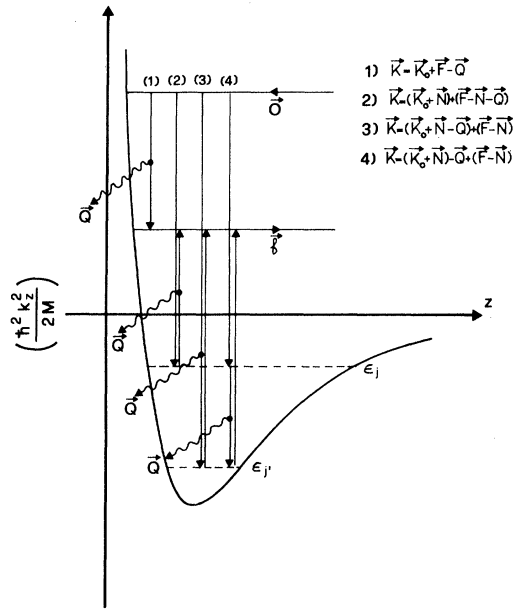

FIG. 6. Perpendicular energies for the most probable (resonant) intermediate states between the incoming $\vec{0}$ and final $\vec{f}$ state of the gas atom. The sketched inelastic process shows four different ways to create one phonon.

graphite and shown in Figs. 3 and 4. The four possible transitions of Eq. (3.20) are sketched in Fig. 6 where: (1) is the direct inelastic transition in the final state $\vec{f}$; (2) is the elastic resonance $(j-\vec{N})$; (3) is the inelastic resonance $(j'-\vec{n})$; while (4) contains the inelastic transition between $(j-\vec{N})$ and $(j'-\vec{n})$.

These few examples show how the proposed theory can explain several relevant effects for selective adsorption on inelastic scattering, where at least three different resonant transitions are important. We will use this theory in the next section to discuss the experimental data of He-graphite. Here it is important to outline how, in a good approximation, all the contributions of the surface dynamics are left in the calculation of $I^0(\vec{f},\vec{0})$ which in general appears as a prefactor. Besides, the resonant contributions can be easily expressed through elastic transition amplitudes $S(\vec{G}-\vec{Q},\vec{G}')$. In this formulation the effects of resonant transitions on inelastic scattering can be identified in a simple way.

IV. DATA ANALYSIS

For a detailed comparison of calculated intensities with experimental data, we recall that the intensity at a given final direction $\Omega_f=(\theta_f,\phi_f)$ is

$$I(\theta_f,\theta_0)=\int_{\omega_f(\vec{Q})} I(\vec{f},\vec{0})\,dE \ , \tag{4.1}$$

with the integral taken along a family of phonons $\omega_f(\vec{Q})$ defined by Eqs. (1.1) and (1.2); for in-plane scattering ($\phi_f=\phi_0$) the line $\omega_f(\vec{Q})$ is the parabola

$$2M\omega_f(\vec{Q})/\hbar=k_0^2-(\vec{K}_0+\vec{F}-\vec{Q})^2/\sin^2\theta_f \ . \tag{4.2}$$

The $I(\vec{f},\vec{0})$ in Eq. (4.1) can be expressed by Eq. (3.20) and the integral evaluated. This calculation is very complicated, mainly because the nonresonant contribution $I^0(\vec{f},\vec{0})$ has to be computed for a lot of phonons. We have seen, however, that for given θ_0 and θ_f, X is constant while the quantities B, B', and C are smoothly varying functions, which can be assumed as constant in the region of integration. If we also assume that $x=\text{const}$, the resonant contribution of Eq. (3.20) can be taken out of the integral. This last assumption ($x=\text{const}$) is in general not true along the integral line $\omega_f(\vec{Q})$ of Eq. (4.2); however in the experimental condition of He-graphite [with $\vec{F}=\vec{0}$ and $\vec{N}=(01)$ and (10)] the family of phonons which gives a constant resonant contribution $[\omega_{N_j}(\vec{Q})]$ lies on a curve of the dispersion plane rather close to the kinematic curve $\omega_f(\vec{Q})$. Then we can substitute x in the integral with the value x^* calculated for the most probable phonon which resonantly contributes at θ_f, while the resonant term of Eq. (3.20) can be taken out of the integral, giving

$$I(\theta_f,\theta_0)\simeq\left|1+\frac{iB}{X+i}+\frac{iC}{x^*+i}+\frac{i^2B'}{(x^*+i)(X+i)}\right|^2 \times\int_{\omega_f(\vec{Q})} I^0(\vec{f},\vec{0})\,dE \ . \tag{4.3}$$

Equation (4.3) is similar to Eq. (3.20) of Sec. III, thus the considerations given for $I(\vec{f},\vec{0})$ of Eq. (3.20) now apply directly to the shape of the angular distribution $I(\theta_f,\theta_0)$, which contains a nonresonant term modulated by three resonant contributions. In fact Eq. (4.3) predicts elastic resonance at selected incident angles θ_0 where $X\simeq 0$; such resonance affects both the elastic diffraction peaks and the neighboring inelastic tails practically in the same way. It also predicts that at any θ_0 a phonon-assisted resonance gives relevant contribution when $x^*\simeq 0$; this inelastic resonance appears as a structure in the angular distribution at the scattering angle θ_j^* at which the contribution of phonons of $\omega_{N_j}(\vec{Q})$ is predominant. Thus the position θ_j^* of the resonant structure in the inelastic scattering identifies, through Eqs. (4.2) and (1.5) the most probable angular frequency ω_q^* and parallel momentum $\vec{Q}^*$ of phonons which give phonon-assisted resonance at each θ_0. The general trend of the experimental data agrees with this description. For a more detailed comparison of ex-

periments with theory, we can write Eq. (4.3) as

$$I(\theta_f,\theta_0)\simeq\left|1+\frac{iB}{X+i}\right|^2\left|1+\frac{iD}{x^*+i}\right|^2\int_{\omega_f(\vec{Q})}I^0(\vec{f},\vec{0})\,dE$$

$$=\mathcal{I}^0(\theta_f,\theta_0)\left|1+\frac{iD}{x^*+i}\right|^2 , \qquad (4.4)$$

where

$$D=C\{1-i[B-(B'/C)]/(X+i+iB)\}$$

is a large quantity at incident angles where $X\simeq 0$. This explains in a qualitative way the large maxima observed with He-graphite.

The functional dependence described by Eq. (4.4) should be adequate in order to study the inelastic structures in the experimental data. Let us define the ratio of resonant to direct inelastic scattering intensity

$$f(\theta_f,\theta_0)=[I(\theta_f,\theta_0)-\mathcal{I}^0(\theta_f,\theta_0)]/\mathcal{I}^0(\theta_f,\theta_0) \qquad (4.5)$$

Then Eq. (4.4), with $x^*=\alpha(\theta_f-\theta_j^*)$ and $D=D_1+iD_2$, gives

$$f(\theta_f,\theta_0)=\frac{D_1^2+D_2^2+2D_1+2D_2\alpha(\theta_f-\theta_j^*)}{1+\alpha^2(\theta_f-\theta_j^*)^2} . \qquad (4.6)$$

This function, which contains four parameters D_1, D_2, α, and θ_j^*, has been used to describe the experimental shape of inelastic resonances near $\theta_f\simeq 57.2°$. Some examples of the best-fit $f(\theta_f,\theta_0)$ curves to the experimental points are shown in Fig. 7; the best-fit parameters were obtained by fixing the position and intensity of maxima, minima, and zeros of the experimental curves. Using this procedure, values for the four parameters of $f(\theta_f,\theta_0)$ were obtained at each θ_0.

The parameter θ_j^*, which defines the position of the resonance, was used to obtain the ω_q^* and $\vec{Q}^*$ of the phonon created at each θ_0. The results are shown in Fig. 8, and compared with the lower branches of dispersion relation for phonons in the hexagonal plane of graphite.[29,30] The points show a large spread, as one may expect because of the uncertainty in the position of the resonance (an error of ±4′ in θ_j^* gives the error bar reported in the figure). In any case the $(\vec{Q}^*,\omega_q^*)$ relation for phonons at the surface seems to be similar to the transverse-acoustical (TA) mode of the bulk. A quite surprising result however is that mainly backward phonons are created in the interaction of He-graphite, at least in the phonon-assisted resonant process. This momentum exchange of the atom with the surface is somewhat unexpected; further measurements are necessary to verify whether this kind of inelastic process depends on the kinematic condition of the experiment or it is a peculiarity of the He-graphite interaction.

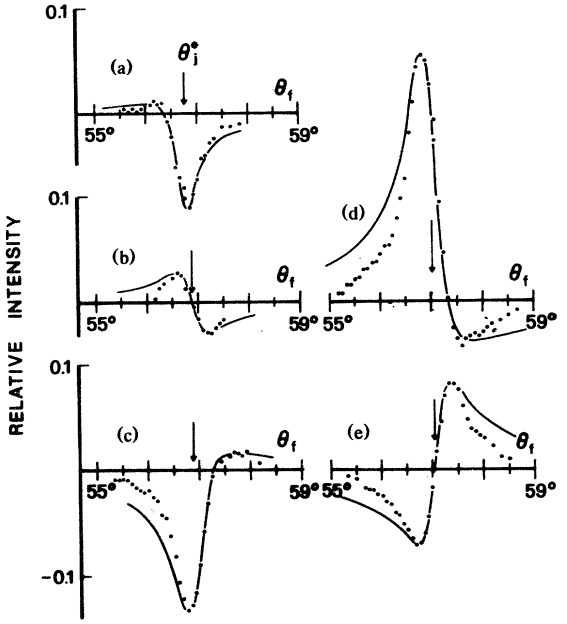

FIG. 7. The ratio $f(\theta_f,\theta_0)$ of resonant to direct inelastic scattering intensity vs the scattering angle θ_f for some incident angles: (a) $\theta_0=43.7°$; (b) $\theta_0=47.7°$; (c) $\theta_0=48.7°$; (d) $\theta_0=51.03°$; and (e) $\theta_0=51.7°$. Dots are experimental points; curves are estimated best-fit functions, with the resonance positions θ_j^* indicated by vertical arrows.

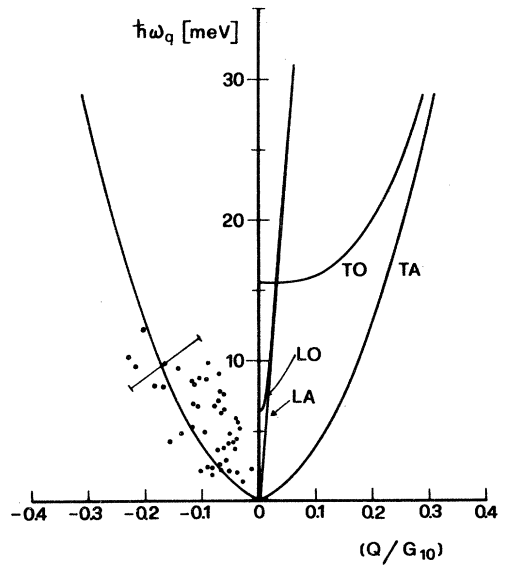

FIG. 8. Mean frequency ω_q^* and parallel momentum $\vec{Q}^*$ of phonons which give phonon-assisted resonances for He-graphite in the $\phi_0=30°$ direction, compared with the lower branches of the phonon dispersion relation in the (0001) direction of the bulk (see Refs. 28 and 29). The error bar represents an error of ±4′ in the position of the resonance.

The values of the second parameter α do not show a clear dependence on θ_0; from the definition of x^* the $\alpha = 2(d\epsilon_n/d\theta_f)/\Gamma_n$ is related to the inverse of the resonance width Γ_n. In the experimental conditions, however, both the energy spread of phonons which contribute to resonance, and the multiphonon processes mask the natural width; thus the experimental value $\alpha = 3.2 \pm 0.4$ (degree $\times$meV^{-1}) has very little meaning.

The last two parameters, namely, the real (D_1) and imaginary (D_2) coefficient of the inelastic resonance amplitude obtained from the experimental data are reported in Fig. 9. Their resonant trend can be used to test the validity of the simple theory of Sec. III. To explain the experimental result, D_1 and D_2 were computed in the Kirchhoff approximation. To be specific, at any incident angle the most probable phonon was selected assuming a dispersion relation $\omega_q^* = vQ^*$, with an average velocity of sound $v = 1.5 \times 10^4$ m sec^{-1}. Then the scattering amplitudes $S(\vec{G} - \vec{Q}^*, \vec{G}')$ which appear in B, B', and C were computed using a hard corrugated wall[28] as:

$$S(\vec{G} - \vec{Q}^*, \vec{G}') = \frac{e^{-W}}{a^2} \int_{\text{unit cell}} d\vec{R} \times \exp[-i(\vec{G} - \vec{Q}^* - \vec{G}') \cdot \vec{R} - i(p_{G-Q^*} + p_{G'})\zeta(\vec{R})] \ , \tag{4.7}$$

the surface profile being given by

$$\zeta(x,y) = 2\zeta_{10}\{\cos(2\pi x/a) + \cos(2\pi y/a) + \cos[2\pi(x-y)/a]\} \ , \tag{4.8}$$

with $\zeta_{10} = -0.023$ Å.[31] Both the Debye-Waller coefficient W and the perpendicular momentum transfer p_{G-Q^*} were calculated by assuming a well depth $D = 15.7$ meV.[5] The values of Γ_N and Γ_n were roughly taken from the elastic resonances.[5,18]

The result of these calculations is shown in Fig. 10; both $D_1(\theta_0)$ and $D_2(\theta_0)$ show a superposition of a nonresonant negative term, plus resonant structures with a maximum followed by a narrow minimum for each energy level ϵ_j of the attractive well. These appearances of the theoretical amplitudes are in qualitative agreement with the experimental behavior shown in Fig. 9, where the oscillations are obviously quenched. Also the relative height of experimental maxima seems correctly predicted by the theory. The most relevant discrepancy between the calculation and the experimental data amounts to a positive background which should be added to the theoretical $D_1(\theta_0)$ value. This defect can probably be attributed to a partial failure of the factorization assumption of Eq. (3.15) which indeed holds only in the simplest case, where the impinging atom transfers momentum to one surface atom only.

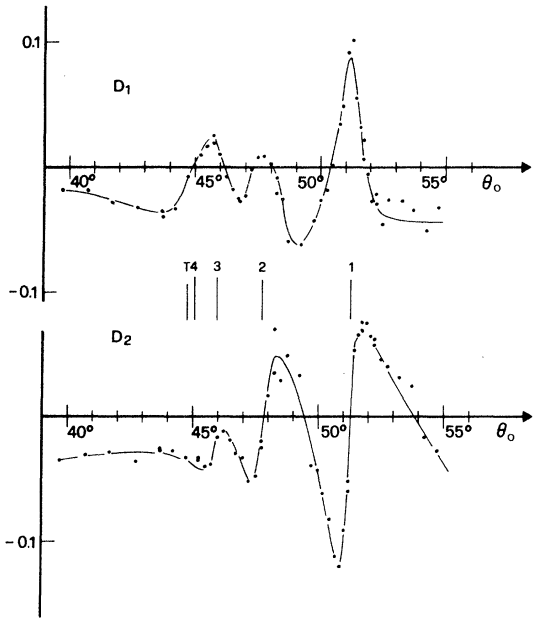

FIG. 9. Best-fit experimental values for the real D_1 and imaginary D_2 coefficient of the inelastic resonance amplitudes vs the incident angle θ_0. Vertical lines indicate elastic resonance positions.

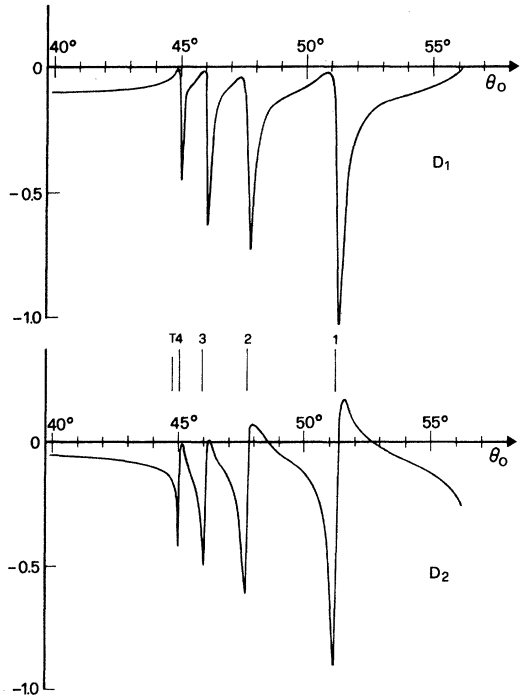

FIG. 10. Inelastic resonance amplitude $D = D_1 + iD_2$ calculated in the Kirchhoff approximation using a hard corrugated wall potential.

The qualitative agreement obtained in the Kirchhoff approximation is a strong indication that the proposed theory, even in the simplified model of Eq. (3.20), can correctly explain the resonance structures in the inelastic scattering, although a more refined model would be required to reproduce the experimental results in details.

V. SUMMARY AND DISCUSSION

We have tried to explain the resonance structures observed in the inelastically scattered angular distributions; the theory presented in Sec. III can be considered as the first attempt of "true" inelastic calculations regarding selective adsorption processes. Although the role of inelastic effects at resonances was previously believed to be theoretically a very difficult problem, we have shown that the occurrence of maxima or minima in the inelastic scattering can be explained in simple terms. Much guidance in developing a theory for the single-phonon resonant scattering was provided by the basic work of Celli, Garcia, and Hutchison[18] on the elastic resonant diffraction. Explicit formulas for the inelastic scattering were obtained in the semiclassical or eikonal approximation,[28] with a corrugated time-dependent hard wall. All the selective adsorption effects observed in the inelastic scattering of He-LiF and Ne-LiF (Refs. 12 and 13) are in qualitative agreement with such a model. We computed the inelastic resonance amplitude for different incident conditions for He-graphite; a direct comparison with the experimental data shows a nearly quantitative agreement. All these features seem to confirm the outlines of the proposed inelastic scattering calculation. The explanations obtained from a semiclassical theory are especially appealing because of their simplicity.

Although the more relevant effort of the present study was devoted to a better understanding of resonance structures in the inelastic scattering, we obtained also some information on the graphite surface dynamics. We used kinematic conditions Eqs. (1.5) and (4.2) to identify phonons without energy analysis. The result shows, still with a large uncertainty, a dispersion relation for the most probable created phonons which is in agreement with the knowledge on the dynamics of the bulk.[29,30] A surprising result was that the inelastic scattering of He-graphite mainly created backward phonons, at least in the phonon-assisted resonances. This result must be considered as preliminary; it awaits confirmation from measurements in different experimental conditions. Detailed measurements of in-plane and out-of-plane angular distributions of inelastic scattering at selective adsorption probably must be coupled with energy analysis of the scattered particles.

Finally we would like to present a few comments on the double-resonance transition process we have seen to be responsible for large maxima in the inelastic tails of He-graphite scattering peaks. The effect, not yet observed till now, seems to reply to the common question on where the intensity subtracted to the elastic peaks goes in a selective adsorption process. The need of an optical potential[21–23] showed that, as originally suggested by Lennard-Jones and Devonshire,[32] inelastic processes are enhanced during the resonant motion of He atoms near the surface of a solid. We have confirmed this, showing also that, among other things, inelastic transition between different energy levels of the potential well plays a very important role. Going beyond the limits of single phonon theory, we can suppose that a cascade of resonant inelastic transitions between energy levels correspond to the enhancement of inelastic scattering, that was thought originally[32] to be the sole cause of selective adsorption.

ACKNOWLEDGMENTS

It is a pleasure for the authors to express their gratefulness to A. C. Levi, G. Boato, A. M. Marvin, and V. Celli for several helpful discussions and comments.

[1] M. J. Cardillo and G. E. Becker, Phys. Rev. Lett. 40, 1118 (1978); 42, 504 (1979).
[2] G. Boato, P. Cantini, and R. Colella, Phys. Rev. Lett. 42, 1635 (1979); Physica (Utrecht) 99B+C, 59 (1980).
[3] K. H. Rieder and T. Engel, Phys. Rev. Lett. 43, 373 (1979).
[4] G. Derry, D. Wesner, W. Carlos, and D. R. Frankl, Sur Sci. 89, 629 (1979).
[5] G. Boato, P. Cantini, C. Guidi, R. Tatarek, and G. P. Felcher, Phys. Rev. B 20, 3957 (1979).
[6] E. Ghio, L. Mattera, C. Salvo, F. Tommasini, and U. Valbusa, J. Chem. Phys. 73, 556 (1980).
[7] J. M. Horne and D. R. Miller, Phys. Rev. Lett. 41, 511 (1978).
[8] B. Feuerbacher, M. A. Adriaens, and H. Thuis, Surf. Sci. 94, L171 (1980).
[9] G. Brusdeylins, R. B. Doak, and J. P. Toennies, Phys. Rev. Lett. 44, 1417 (1980); in *Proceedings of the Third European Conference on Surface Science, Cannes, 1980,* edited by D. A. Degras and M. Costa, Supplement No. 201 à la Revue "Le Vide, Les Couches Minces" (Société Française du Vide, Paris, 1980).
[10] G. Benedek, Surf. Sci. 61, 603 (1976).
[11] T. S. Chen, F. W. de Wette, and G. P. Alldredge, Phys. Rev. B 15, 1167 (1977).

[12]B. R. Williams, J. Chem. Phys. 55, 1315 (1971).
[13]P. Cantini, G. P. Felcher, and R. Tatarek, Phys. Rev. Lett. 37, 606 (1976); Surf. Sci. 63, 104 (1977).
[14]H. Frank, H. Hoinkes, and H. Wilsch, Surf. Sci. 63, 121 (1977).
[15]H. Chow and E. D. Thompson, Surf. Sci. 54, 269 (1976); 59, 225 (1976).
[16]C. E. Harvie and J. H. Weare, Phys. Rev. Lett. 40, 187 (1978); K. Wolfe and J. H. Weare, *ibid.* 41, 1663 (1978).
[17]N. Garcia, V. Celli, and F. O. Goodman, Phys. Rev. B 19, 634 (1979).
[18]V. Celli, N. Garcia, and J. Hutchison, Surf. Sci. 87, 112 (1979).
[19]H. U. Finzel, H. Frank, H. Hoinkes, M. Luschka, H. Nahr, H. Wilsch, and U. Wonka, Surf. Sci. 49, 577 (1975).
[20]D. R. Frankl, D. Wesner, S. V. Krishnaswamy, G. Derry, and T. O'Gorman, Phys. Rev. Lett. 41, 60 (1978).
[21]N. Garcia, W. E. Carlos, M. W. Cole, and V. Celli, Phys. Rev. B 21, 962 (1980).
[22]H. Chow and E. D. Thompson, Surf. Sci. 82, 1 (1979).
[23]K. L. Wolfe and J. H. Weare, Surf. Sci. 94, 581 (1980).
[24]D. Wesner, G. Derry, G. Vidali, T. Twaites, and D. R. Frankl, Surf. Sci. 95, 367 (1980).
[25]N. Garcia, J. Garcia-Sanz, and J. Solana, J. Chem. Phys. 66, 4694 (1977).
[26]H. Chow, Surf. Sci. 66, 22 (1977).
[27]R. Manson and V. Celli, Surf. Sci. 24, 495 (1971).
[28]A. C. Levi, Nuovo Cimento B 54, 357 (1979).
[29]R. Nicklow, N. Wakabayashi, and H. G. Smith, Phys. Rev. B 5, 4951 (1972).
[30]K. K. Mani and R. Ramani, Phys. Status Solidi 61, 659 (1974).
[31]G. Boato, P. Cantini, and R. Tatarek, Phys. Rev. Lett. 40, 887 (1978).
[32]J. E. Lennard-Jones and A. F. Devonshire, Proc. R. Soc. London Ser. A 156, 6, 29, 37 (1936); 158, 242, 253 (1937).